PNAS RESEARCH ARTICLE | GENETICS

Maternal genetic variants in kinesin motor domains prematurely increase egg aneuploidy

Leelabati Biswas[a,b,c,1], Katarzyna M. Tyc[a,b,1,2], Mansour Aboelenain[a,b,d], Siqi Sun[a,b], Iva Dundović[e], Kruno Vukušić[e], Jason Liu[a], Vanessa Guo[f], Min Xu[g], Richard T. Scott Jr.[h], Xin Tao[f], Iva M. Tolić[e], Jinchuan Xing[a,b,3], and Karen Schindler[a,b,3]

Affiliations are included on p. 11.

Edited by Thomas Spencer, University of Missouri, Columbia, MO; received July 26, 2024; accepted September 27, 2024

The female reproductive lifespan is highly dependent on egg quality, especially the presence of a normal number of chromosomes in an egg, known as euploidy. Mistakes in meiosis leading to egg aneuploidy are frequent in humans. Yet, knowledge of the precise genetic landscape that causes egg aneuploidy in women is limited, as phenotypic data on the frequency of human egg aneuploidy are difficult to obtain and therefore absent in public genetic datasets. Here, we identify genetic determinants of reproductive aging via egg aneuploidy in women using a biobank of individual maternal exomes linked with maternal age and embryonic aneuploidy data. Using the exome data, we identified 404 genes bearing variants enriched in individuals with pathologically elevated egg aneuploidy rates. Analysis of the gene ontology and protein–protein interaction network implicated genes encoding the kinesin protein family in egg aneuploidy. We interrogate the causal relationship of the human variants within candidate kinesin genes via experimental perturbations and demonstrate that motor domain variants increase aneuploidy in mouse oocytes. Finally, using a knock-in mouse model, we validate that a specific variant in kinesin KIF18A accelerates reproductive aging and diminishes fertility. These findings reveal additional functional mechanisms of reproductive aging and shed light on how genetic variation underlies individual heterogeneity in the female reproductive lifespan, which might be leveraged to predict reproductive longevity. Together, these results lay the groundwork for the noninvasive biomarkers for egg quality, a first step toward personalized fertility medicine.

aneuploidy | meiosis | kinesin | oocyte | infertility

Significance

This study presents an enhanced statistical and functional genetic pipeline to identify genetic determinants of reproductive aging linked to egg aneuploidy by analyzing maternal exomes. It demonstrates that variants in kinesin genes, specifically *KIF18A* and *KIF20A*, contribute to increased aneuploidy and accelerated reproductive aging and provide biological validation of a candidate clinical variant for causation of egg aneuploidy. Identification of precision genetic biomarkers for EEA could provide a personalized approach to fertility care, bringing a much-desired genomic medicine lens to fertility treatment.

Female fertility lies at the interface of multiple, complex organ systems and interwoven hormonal axes, all of which are governed by many genes (1, 2). At the convergence of this interplay is the egg. A female must have eggs of sufficient quantity and quality (*i.e.*, biological functionality) to successfully reproduce. One aspect of egg quality, known as egg euploidy—the presence of a correct chromosome complement—is a sine qua non for fertility and reproduction. Euploid eggs, once fertilized, can give rise to developmentally competent embryos, while aneuploid eggs typically cause a failure to implant or early miscarriage (3–5).

Currently, maternal age is the only clinical predictive biomarker for egg euploidy. Aging eggs lose chromosomal cohesion proteins that protect egg euploidy (6–9). As a result, age-dependent increases in egg aneuploidy taper the human female reproductive lifespan beginning in the early thirties and culminating to a near total loss of reproductive potential by the mid-forties, on average, prior to the normal onset of menopause (10, 11). However, there is considerable interindividual heterogeneity in female fertility and female reproductive lifespans (12). Recent studies examining age at natural menopause and female fertility further underscore that maternal genetic variants may contribute to this heterogeneity (13).

Elevated egg aneuploidy (EEA), a form of accelerated reproductive aging in which individuals have higher egg aneuploidy than expected for their maternal age, is a particular example of a pathological phenotypic variation affecting female fertility (14). The genetic basis of EEA is poorly understood, and the identification of causal genetic variants for EEA has been challenging for several reasons. First, egg aneuploidy phenotype data linked with maternal genetic sequencing information are limited. Assessment of an individual's egg aneuploidy status can only occur in a fertility clinic, where the primary focus is on assisting with reproduction rather than investigating underlying causes. Consequently, patients undergoing this protocol do not routinely receive concurrent high-resolution genome or exome sequencing, which explains the rarity of linked genetic-phenotype data. Second, egg aneuploidy is a complex trait that arises from both normal age-dependent changes in eggs and genetic mechanisms. As a result, biologically validating specific genetic

Author contributions: L.B., K.M.T., M.A., S.S., I.D., K.V., I.M.T., J.X., and K.S. designed research; L.B., K.M.T., M.A., S.S., I.D., and X.T. performed research; V.G., M.X., R.T.S., and X.T. contributed new reagents/analytic tools; L.B., K.M.T., M.A., S.S., I.D., K.V., and J.L. analyzed data; and L.B., K.M.T., M.A., S.S., and I.D. wrote the paper.

The authors declare no competing interest.

This article is a PNAS Direct Submission.

Copyright © 2024 the Author(s). Published by PNAS. This article is distributed under Creative Commons Attribution-NonCommercial-NoDerivatives License 4.0 (CC BY-NC-ND).

[1]L.B. and K.M.T. contributed equally to this work.

[2]Present address: Department of Biostatistics and Massey Comprehensive Cancer Center Bioinformatics Shared Resource Core, Virginia Commonwealth University, Richmond, VA 23219.

[3]To whom correspondence may be addressed. Email: jinchuan.xing@rutgers.edu or ks804@hginj.rutgers.edu.

This article contains supporting information online at https://www.pnas.org/lookup/suppl/doi:10.1073/pnas.2414963121/-/DCSupplemental.

Published October 30, 2024.

Downloaded from https://www.pnas.org by 188.129.80.218 on July 30, 2025 from IP address 188.129.80.218.

variants requires complex, multipronged model systems that combine multiple factors, such as advanced age and genetic variation. Therefore, the elucidation of the maternal genetic determinants of egg aneuploidy remains scarce to date.

Here, we overcome these limitations through a comprehensive multidisciplinary approach. Using a bioinformatic strategy, we identify genes associated with EEA. By extending to experimental approaches in mice, we unravel the roles of molecular motor proteins called kinesins in maintaining egg euploidy and shaping reproductive aging. Kinesins are a superfamily of 14 classes of oligomeric motor proteins that bind microtubules, usually have plus-end directed movement, and share a common motor domain (15–17). We report human variants in kinesin genes *KIF20A* and *KIF18A* associated with pathological EEA. KIF20A is a dimeric kinesin that transports the chromosomal passenger complex (CPC) in mitosis and meiosis, a function important for faithful chromosome segregation (18–23). KIF18A regulates microtubule dynamics, and aneuploid cells are uniquely sensitive to its loss (24–26). We experimentally examined variants from human patients in mouse oocytes and show that they perturb meiosis and elevate meiotic aneuploidy. Our findings not only offer insight into the basis of heterogeneity in reproductive aging but also provide opportunities for leveraging these mechanisms to optimize reproductive health across the female lifespan.

Results

Patient Description and Data Quality. We previously collected deidentified maternal age and embryonic aneuploidy data from 753 White, non-Hispanic patients treated at Reproductive Medicine Associates of New Jersey. Using a robust nonlinear regression analysis, we selected 182 patients who had either high (43% to 100%; average 67%) or low (0% to 50%; average 11.1%) aneuploidy rate relative to their maternal ages. Whole-exome sequencing was performed on the 182 patients, with subsequent quality control checks for excess heterozygosity and consistency between exome-derived and self-reported race estimates (*Materials and Methods* for detail). This resulted in 178 patients with extreme aneuploidy rates (93 high, 85 low) being included in the association studies, as previously described (27) (Fig. 1*A*). The patients' ages ranged from 24 to 43 y with a median of 37 y. The low-aneuploidy group had a median age of 37 y (IQR: 34-39) and the high-aneuploidy group had a median age of 36 y (IQR: 33-39). Here, we analyzed 494,448 variant sites, including 441,457 single nucleotide variants (SNVs) and 52,991 insertions/deletions (INDELs) (Dataset S1).

VAAST and Gene Ontology Analyses Implicate Kinesins in EEA. First, we used the program VAAST (28) to identify potentially causal variants in EEA patients. A total of 8,611 genes had positive scores, but no single gene achieved a genome-wide significance level. To assess the relevance of the genes that were prioritized by VAAST, we manually reviewed the top 50 genes for known mouse phenotypes reported in MouseMine (29). Out of the 50 genes, phenotypes reported in MouseMine for 13 genes were highly relevant in the context of this study (infertility, embryonic defects, prenatal lethality, *etc.*) (*SI Appendix*, Table S2). This preparatory step suggests that the top candidates from our analyses were indeed related to reproductive disease. To further prioritize the candidate genes, we evaluated the top VAAST genes with an assigned *P*-value < 0.05 (n = 404 genes, *SI Appendix*, Table S2) for enriched gene ontology (GO) terms using the online tool ConsensusPathDB (CPDB). The GO cellular compartment (CC) terms such as "microtubule" (19 genes) and "kinesin complex" (5 genes) were the two most statistically significantly enriched GO CC terms ($q < 0.05$). All 5 genes from "kinesin complex" were among the 19 "microtubule" genes (*KIF18A, KIF5C, KIF16B, KIF20A,* and *KLC1*) (Fig. 1*B*). *SI Appendix*, Table S3 for a complete list of gene lists and associated terms.

To further explore the interaction among the candidate genes, we constructed a protein–protein interaction (PPI) network using information from three common databases (CPDB, STRING, and GIANT). Among the 404 genes, 107 formed a connected network (*SI Appendix*, Fig. S1 and Table S4), including several genes that have an association with female aneuploidy (Known_genes, blue, *SI Appendix*, Fig. S1), or predicted to be associated with meiosis in humans by Meiosis Online (MO_human, orange, *SI Appendix*, Fig. S1), including *KIF18A, FANCA, and KAT6A*. To further identify biologically relevant functional units, we applied the PAPER algorithm (30), which identifies root nodes and functional modules within a network. With this method, we identified seven discrete modules within the PPI network (Fig. 1*C*), and we identified GO terms enriched in these modules (*SI Appendix*, Table S5). Within module 2, five genes (*KIF20A, CIT, ANLN, NCAPG2,* and *KIF18A*) belong to the mitotic cell cycle process group (GO:1903047). Two of the five genes, *KIF18A* and *KIF20A*, are members of the kinesin superfamily of proteins (KIFs) identified in the VAAST-GO pipeline. We prioritized these two genes for validation studies because they overlapped between the VAAST-GO and the PPI approaches described here (also illustrated in Fig. 1*B*). Prior to conducting validation studies, we confirmed that these kinesins are expressed in mouse oocytes. Previous studies indicated KIF20A spindle localization in mouse and porcine oocytes (31, 32) which we verified here (*SI Appendix*, Fig. S2*A*). We found that KIF18A also localized to the Metaphase I spindle, consistent with previous reports in mitotic and meiotic cells (25, 33–35) (*SI Appendix*, Fig. S2*B*).

Motor Domain Inhibition in Candidate Kinesins Increases Egg Aneuploidy. After identifying four variants in *KIF20A* and two in *KIF18A* that are enriched in EEA patients compared to low-aneuploidy controls, we sought to prioritize these variants for experimental validation based on their potential functional significance (Fig. 1*D*). Both KIF genes have motor domains, the enzymatic regions with dynamic microtubule-binding affinity and ATP-hydrolysis activity that confer motility to the protein. Each gene contained EEA patient variants within this domain (Fig. 1*D*). To begin to test the hypothesis that the kinesin motor domain mutations could cause EEA, we first determined whether kinesin motor function is important for euploidy. Therefore, we assessed whether biochemical inhibition of each candidate kinesin's motor domain causes egg aneuploidy (Fig. 2*A*). We treated Prophase I oocytes with either Sovilnesib to inhibit KIF18A motor function (36) or Paprotrain to inhibit KIF20A motor function (37). We then cultured the oocytes to metaphase II and performed an in situ chromosome counting assay to evaluate whether each egg was aneuploid or euploid. We found that the frequency of aneuploidy increased significantly in oocytes treated with either Paprotrain or Sovilnesib. Specifically, 52.3% of oocytes were aneuploid in the Paprotrain-treated group, and 40.0% of oocytes were aneuploid in the Sovilnesib-treated group, compared with 15.9% and 20.8% aneuploidy in oocytes treated with vehicle controls, respectively (Fig. 2 *B* and *C*). These results indicate that kinesin motor activity is required for egg euploidy and that impairment of this function can lead to egg aneuploidy.

Kinesin Variants Enriched in EEA Patients Increase Egg Aneuploidy. Having determined that the kinesin motor domain is required for egg euploidy, we turned our attention to the three

Downloaded from https://www.pnas.org by 188.129.80.218 on July 30, 2025 from IP address 188.129.80.218.

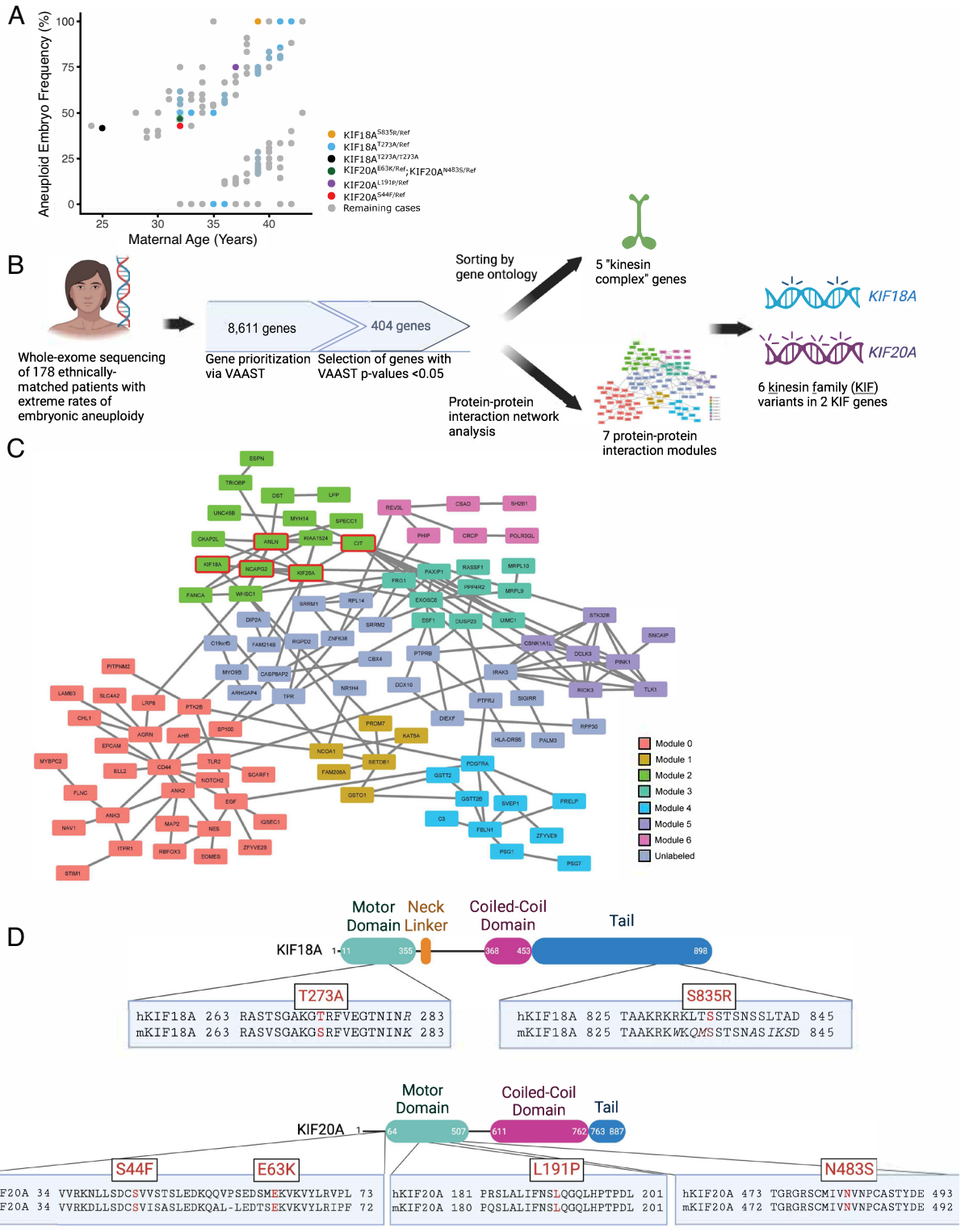

Fig. 1. Bioinformatic approach to identify candidate aneuploidy genes. (*A*) Patient cohort and kinesin variant distribution. Colored dots indicate a genotype encoding the protein variants noted. "Ref" = reference allele. n = 182 patients. Note that in our cohort, both the numerator (aneuploid eggs) and denominator (total eggs collected) are relatively small discrete values with a limited set of possible fractions. As such, some data points overlap because multiple individuals may share the same fraction. *SI Appendix*, Table S1 for a full description of the cohort. (*B*) Bioinformatic prioritization pipeline. Patients were divided into low-aneuploidy and high-aneuploidy cohorts and subjected to exome sequencing. Variants were identified and used for association analysis with VAAST. Genes identified by VAAST were used for gene ontology (GO) enrichment and protein–protein interaction network analyses. Genes that were enriched in the GO term "kinesin complex" and parts of a functional module were selected for functional studies in mouse oocytes. (*C*) Protein–protein interaction network of candidate genes. Genes are color-coded by their module assignments by PAPER. In module 2, genes belonging to the "mitotic cell cycle process" GO term are circled in red. (*D*) Mutation diagram illustrating the protein consequences of EEA-enriched mutations in KIF18A and KIF20A. Local alignments of human KIF18A (hKIF18A) and mouse KIF18A (mKIF18A). Italicized residues are not conserved between the human and mouse. Red, bolded residues are those substituted by an alternative allele in the high-aneuploidy individuals.

kinesin motor domain variants enriched in our EEA patient cohort (Fig. 1*D*). To test the hypothesis that these variants cause EEA by increasing egg aneuploidy, we evaluated each variant for its ability to cause egg aneuploidy when overexpressed in mouse oocytes. We microinjected *Gfp*-tagged cRNA encoding each variant into age-matched, wild-type mouse oocytes arrested in Prophase I, cultured

Downloaded from https://www.pnas.org by 188.129.80.218 on July 30, 2025 from IP address 188.129.80.218.

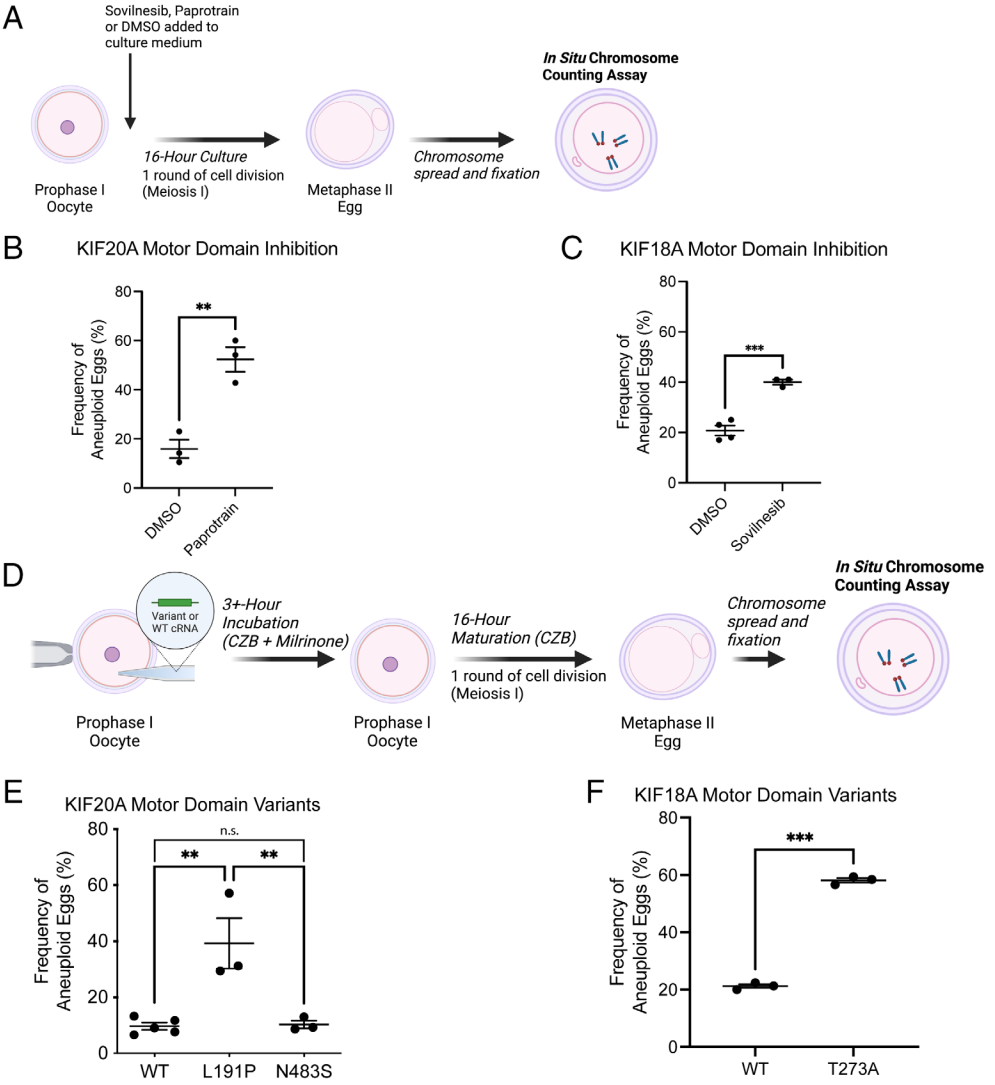

Fig. 2. Evaluation of kinesin motor domains in mouse oocytes. (*A*) Diagram of strategy to chemically inhibit KIF18A (Sovilnesib) or KIF20A (Paprotrain) and assess the frequency of aneuploidy. (*B*) Frequency of aneuploidy in oocytes treated to inhibit KIF20A. DMSO, n = 94 oocytes from 3 mice; 15 μM, n = 120 oocytes from 3 mice. Two-tailed *t* test. $P = 0.0043$. (*C*) Frequency of aneuploidy in oocytes treated to inhibit KIF18A. DMSO, n = 58 from 5 mice; 500 nM, n = 67 from 3 mice. Two-tailed *t* test. $P = 0.0005$. (*D*) Diagram of strategy to express motor domain variants and assess the frequency of aneuploidy. (*E*) Frequency of aneuploidy in oocytes overexpressing *KIF20A* patient variants. One-way ANOVA. WT, n = 39 oocytes from 3 mice; L191P, n = 41 oocytes from 3 mice; N483S, n = 38 oocytes from 3 mice. WT v L191P, $P = 0.0026$; WT v N483S, $P = 0.0058$. (*F*) Frequency of aneuploidy in oocytes overexpressing *KIF18A* variants. Two-tailed *t* test. $P < 0.001$. WT, n = 37 from 3 mice; T273A, n = 35 from 3 mice. Data are represented as mean ± SEM. $*P < 0.05$, $**P < 0.01$, $***P < 0.001$, and $****P < 0.0001$.

the oocytes in vitro to Metaphase of meiosis II (Met II), and performed an in situ chromosome counting assay to determine whether each egg was aneuploid (Fig. 2*D*).

Upon performing the chromosome-counting assay, we observed that oocytes expressing either KIF20A^{L191P} or KIF18A^{T273A} had a significantly higher frequency of egg aneuploidy compared to controls (Fig. 2 E, F). However, expression of the KIF20A^{N483S} motor domain variant did not significantly change aneuploidy frequency relative to controls (Fig. 2*E*). As a control, we confirmed that the exogenous WT and variant proteins were expressed at a similar level by assessing GFP levels by western blotting (*SI Appendix*, Fig. S3). Notably, upon modeling the impact of each variant on protein stability in silico using PoPMuSiC (38), we found that both variants are likely destabilizing, with predicted ΔΔG of +3.15 for KIF20A^{L191P} and +0.81 for KIF18A^{T273A}. Having determined that KIF20A^{L191P} and KIF18A^{T273A} increase egg aneuploidy and are likely pathogenic, we next sought to understand the functional impact of these patient kinesin motor domain variants on eggs.

KIF20A^{L191P} and KIF18A^{T273A} Disturb Critical Processes in Oocyte Meiosis I. Meiosis I is the process by which oocytes prepare to segregate their chromosomes; most egg and embryo aneuploidies arise from errors in meiosis I (3–5). Therefore, to evaluate the functional consequence of each EEA-patient-enriched kinesin motor domain variant on egg quality, we assessed the effect of exogenous expression of the EEA-patient-enriched motor domain variants on meiosis I in detail. We used gene-specific assays to assess the impact of the aneuploidy-causing variants on KIF20A and KIF18A function.

In mitotic cell division, KIF20A binds to and transports the CPC from chromosomes to the spindle midzone during anaphase where the complex then promotes formation of the cleavage furrow and regulates cytokinesis (19–22). This localization is critical for the recognition of lagging chromosomes in anaphase and telophase to delay cell division (23). In these cells, depletion of KIF20A prevents CPC localization to the spindle midzone and midbody (39).

First, we examined the localization of exogenous, GFP-tagged KIF20A to validate the utility of the GFP-tagged construct for functional studies. We microinjected oocytes with either *Gfp*-tagged WT-*hKIF20A* or h*KIF20A*^{L191P}, cultured them for 10 h, fixed them, and labeled for tubulin, to reveal the midbody (Fig. 3 *A* and *B*). The exogenously expressed KIF20A variant localized in the same fashion as the reference allele (Fig. 3*B*). Exogenous KIF20A-GFP localized to Telophase I midbodies (Fig. 3*B*), as reported of endogenous KIF20A in mouse oocytes (40). The localization of hKIF20A-Gfp at midbodies suggests it is competent to move CPC cargo during Telophase I.

In meiotic cells, like mouse oocytes, Aurora kinase C (AURKC) is the catalytic subunit of the CPC (41, 42). To assess whether this function is maintained in oocytes expressing KIF20A^{L191P}, we next evaluated the effect that KIF20A^{L191P} had on AURKC/

Downloaded from https://www.pnas.org by 188.129.80.218 on July 30, 2025 from IP address 188.129.80.218.

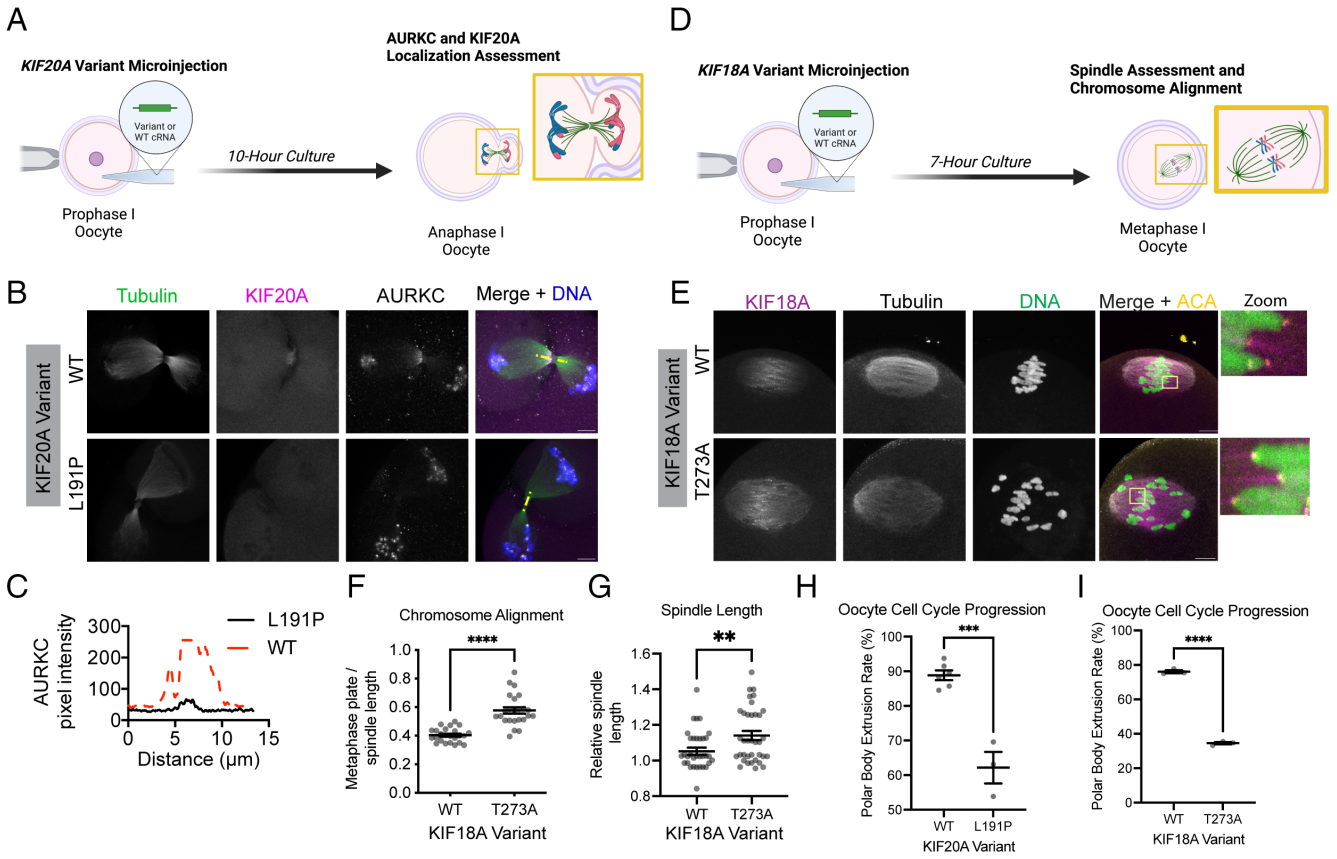

Fig. 3. Functional KIF20A and KIF18A assays in oocytes expressing patient variants. (*A*) Diagram of strategy to assess Telophase I AURKC localization. (*B* and *C*) AURKC signal at the midzone in oocytes expressing variant KIF20A. Oocytes were fixed and immunolabeled for AURKC (gray), α-tubulin (green), and DNA (blue). GFP-hKIF20A, magenta. n > 15 oocytes/group. (*C*) Intensity of AURKC along the yellow line in (*B*). (*D*) Diagram of strategy to assess Metaphase I spindles in oocytes expressing variant KIF18A. (*E*) Metaphase I chromosome alignment images. α-tubulin (gray), ACA (yellow), and DNA (green), hKIF18A (magenta). Zoom-insets of k-fiber tips on the right. (*F* and *G*) Quantifications from *E*. WT, n = 34 oocytes; T273A, n = 36 oocytes. Each dot represents one oocyte. Student's *t* test. (*F*) $P = 0.0003$. (*G*) $P = 0.009$. (*H* and *I*) Frequency of polar body extrusion in oocytes overexpressing *KIF20A* and *KIF18A* variants. Dots represent one replicate. H: WT, n = 94 oocytes; L191 *n* = 92 oocytes. Student's *t* test. $p = 0.002$. I: WT, n = 81 oocytes; T273A, n = 89 oocytes. Student's *t* test. $P < 0.0001$. Data are represented as mean ± SEM. ns, not significant; $^{*}P < 0.05$, $^{**}P < 0.01$, $^{***}P < 0.001$, $^{****}P < 0.0001$. (Scale bars, 5 μm.)

CPC localization at Telophase I. In the oocytes described above, we also probed for AURKC (Fig. 3 *A* and *B*). Oocytes expressing the reference allele (WT) had enriched AURKC in the meiotic midbody at Telophase I (Fig. 3*B*, *Top*). The exogenous hKIF20A colocalized with AURKC in this region (Fig. 3*B*, *Merge*). In contrast, AURKC did not localize to meiotic midbodies and instead remained on chromosomes in oocytes expressing hKIF20A^{L191P} (Fig. 3*B*, *Bottom* and 3C). The failure of the CPC to relocalize was accompanied by loss of hKIF20A^{L191P} localization in this region. We confirmed this phenotype by assessing AURKC meiotic midbody localization in Paprotrain-treated (KIF20A-inhibited) oocytes. AURKC midbody signal decreased in oocytes cultured in 15 μM Paprotrain as compared to vehicle control (*SI Appendix*, Fig. S4). Paprotrain inhibits KIF20A's ATPase function (37). These data indicate that hKIF20A^{L191P} fails to migrate to the midbody along with its cargo, the CPC, and suggest that hKIF20A^{L191P} has altered motor function.

We next assessed KIF18A function in oocytes expressing hKIF18A^{T273A}. KIF18A is a motor protein that promotes chromosome alignment by dampening chromosome oscillation (25, 43). Loss of KIF18A causes chromosome misalignment in mitotic cells, so we assessed this function in oocytes expressing hKIF18A^{T273A}. We microinjected mouse oocytes with cRNA encoding hKIF18A^{T273A}, matured the cells to Metaphase I, and labeled spindles and chromosomes (Fig. 3*D*). We examined the localization of exogenous, GFP-tagged KIF18A and found that the exogenously expressed KIF18A variant localized in the same fashion as the reference allele (Fig. 3*E*). KIF18A-GFP localized similarly to endogenous KIF18A at the Metaphase I spindle (compare Fig. 3*E* to *SI Appendix*, Fig. S2*B*). Of note, KIF18A-GFP demonstrated pronounced accumulation at the kinetochore-fiber tips, similar to a recent report using a transgenic KIF18A-GFP mouse strain (44) (Fig. 3*E*) and consistent with somatic cells' localization of KIF18A (33). Importantly, the GFP tag does not alter subcellular localization. Furthermore, these data suggest that exogenous hKIF18A-GFP and the patient variant are similarly competent as the endogenous protein in their ability to bind to microtubules. Further, the localization at plus-end tips suggests that hKIF18A-GFP and the tested motor domain variants (Fig. 1*D*) are competent to conduct plus-end-directed motor activity. We note that although the tubulin intensity appears reduced in the selected image, analysis of the entire dataset did not find significant difference in tubulin intensity (*SI Appendix*, Fig. S5).

Next, we calculated the ratio between the length of the metaphase plate (the distance between the two farthest chromosomes) and spindle length, as a metric of chromosome alignment. Compared to oocytes expressing the reference allele (WT), we observed an increase in the frequency of chromosome misalignment when oocytes expressed KIF18A^{T273A} (Fig. 3 *E* and *F*). Notably, we also found an increase in spindle length (Fig. 3*G*), a phenotype that also occurs with KIF18A-knockdown (25, 33). KIF18A is a microtubule-stabilizing enzyme and its inactivity in

Downloaded from https://www.pnas.org by 188.129.80.218 on July 30, 2025 from IP address 188.129.80.218.

meiotic and mitotic cells is frequently associated with abnormally long spindles (25, 33, 35, 45). Together, these results suggest that KIF18A function is altered in oocytes expressing hKIF18A^{T273A}.

Errors in meiosis I can lead to meiotic delay or arrest through activation of cell cycle checkpoints (46–48). Therefore, we assessed meiotic progression, as measured by the frequency of polar body extrusion (PBE) after 16 h of culture, in oocytes expressing hKIF20A^{L191P} or hKIF18A^{T273A}. We found a significant reduction in meiotic progression in oocytes expressing hKIF20A^{L191P} (62% PBE vs 89% in WT control; Fig. 3*H*) and hKIF18A^{T273A} (35% PBE vs 76% in WT control; Fig. 3*I*). These results suggest that although some proportion of oocytes expressing kinesin motor domain variants enriched in EEA patients progress through meiosis I to yield aneuploid eggs, another population of these oocytes fails to proceed through cytokinesis in a timely fashion, likely due to errors in meiosis I.

mKIF18A^{S273A} Accelerates Female Reproductive Aging by Prematurely Increasing Egg Aneuploidy. Having validated the causality of hKIF20A^{L191P} and hKIF18A^{T273A} in egg aneuploidy in vitro, we considered the utility of generating preclinical in vivo models of these variants. First, we assessed the allele frequency (AF) of these kinesin motor domain variants in EEA patients as compared with patients with low rates of embryonic aneuploidy. The *KIF20A^{L191P}* allele was present in 1 of 178 patients as a heterozygous with an AF of ~0.0028. In gnomAD, this allele is rare (AF 0.00001533 in the European non-Finnish population). Because this allele is very rare in the general population and therefore has restricted impact potential, we elected not to generate a mouse model of this variant. In contrast, we found that hKIF18A^{T273A} was present in 17 out of 178 patients with an AF of ~0.05 (Fig. 1*A*, blue dots). The same allele was found at a similarly high AF in the gnomAD database for the European non-Finnish population (0.03881), indicating this is a relatively common variant. In our cohort, hKIF18A^{T273A} heterozygosity is strongly associated with the high-rate group (13 HRG patients, and only 3 LRG patients), and one patient, a 25-year-old with 45% aneuploidy, is homozygous (Fig. 1*A*, black dot).

Having established that h*KIF18A^{T273A}* is a common allele that is both enriched in EEA patients and functionally pathologic to mouse eggs in vitro, we sought to establish a preclinical in vivo model of h*KIF18A^{T273A}*. We generated a knock-in mouse model by using CRISPR/Cas9 genome editing to replace the mouse codon TCA that encodes Serine 273 in *Kif18a* with a CGC encoding Alanine (*SI Appendix*, Fig. S6). This mouse model provided two opportunities: 1) validate the variant as a genetic cause of EEA in an in vivo, mammalian context; 2) assess the functional impact of the variant on whole-organism fertility and endogenously expressing mammalian eggs.

To evaluate the consequence of harboring the KIF18A^{S273A}-encoding allele on female fecundity, we performed fertility trials in which female mice of each *Kif18a* genotype were paired with highly fertile B6D2/J males for six months and assessed for litter size over time. At reproductively young ages (~2 mo of age), WT, heterozygous, and homozygous mutant dams were similarly fertile ($P > 0.9999$; Fig. 4 *A* and *B*). However, after five months of age, the litter sizes of homozygous mutant dams were significantly smaller, compared with WT dams ($P = 0.0425$). As a result, over the whole trial, homozygous mutant mice had significantly different fertility from WT mice ($P = 0.0009$; Fig. 4*A*). We note that ovaries collected after the trial from 6-month-old homozygous mice had similar follicle counts to WT littermates, indicating that decreased ovarian reserve did not contribute to the subfertility (*SI Appendix*, Fig. S7). This finding contrasts with another mouse model bearing a *Kif18a* allele, in which female mice demonstrate subfertility resulting from a severely reduced ovarian reserve (49). We concluded that the female subfertility phenotype of KIF18A^{S273A}-encoding mice arises only in the context of moderately increased maternal age, suggesting an acceleration of the typical murine age-dependent decline in fertility (50).

It is likely that the effect of the variant is sex- and meiosis-specific. Litter sizes were not significantly different between *Kif18a* variant males ($P = 0.065$; *SI Appendix*, Fig. S8), indicating that the effect of *Kif18a^{S273A}* on fertility is specific to females. In addition, mitotic chromosome segregation was unaffected by *KIF18A^{T273A}* when expressed in somatic U2OS cells, both in terms of chromosome alignment ($P = 0.559$; *SI Appendix*, Fig. S9 *A* and *B*) and chromosome segregation errors ($P = 0.465$; *SI Appendix*, Fig. S9*C*). hKIF18A^{T273A} accumulated at the plus-end tips of microtubules throughout mitosis in U2OS cells, with a statistically significant but modest 6% decrease in accumulation compared to hKIF18A^{WT} ($P = 0.0193$, T273A 0.840 v. WT 0.893; *SI Appendix*, Fig. S9 *D–E*). Further studies examining the relationship between *KIF18A^{T273A}*, sex, aging, and other body systems are required to fully elucidate the consequences of the variant on both male mammals and somatic tissues.

Having established that *Kif18a^{S273A}* exacerbates the age-dependent decline in female fertility, we next asked whether egg aneuploidy caused this decline. We assessed egg aneuploidy at the age at which fertility was similar (~9 wk of age, young) and at the age at which intergenotype fertility diverged (~20 wk of age, older). In young mice, the proportion of aneuploid eggs trended upward in homozygous mutant mice but was not significantly different from WT mice (Fig. 4*C*; 23% vs 8%; $P = 0.059$). In older mice, aneuploidy was significantly higher in homozygotes, compared with controls (Fig. 4*C*; 50% vs 13%; $P = 0.008$). To identify the mechanism by which *Kif18a^{S273A}* causes egg aneuploidy, we examined kinetochore–microtubule attachments, a key cause of aneuploidy, in oocytes collected from older (20-wk-old) *Kif18a$^{S273A/S273A}$* mice. We treated these oocytes with a brief incubation in ice-cold media to depolymerize microtubules not stably attached to kinetochores. We analyzed ~1,000 kinetochores per genotype and found a significant increase in unattached kinetochores in oocytes from aged *Kif18a^{S273A}* mice compared to age-matched WT controls (Fig. 4 *D* and *E*; 16.1% vs 5.5% $P < 0.0001$). This defect may result from altered KIF18A-mediated microtubule dynamics at the microtubule K-fiber tip.

Collectively, these data demonstrate that *KIF18A^{S273A}* specifically increases egg aneuploidy and that the effect of KIF18A^{S273A} on egg aneuploidy is compounded by maternal age-dependent changes in the egg. Altogether, the data support a model in which KIF18A^{S273A} migrates to the k-fiber tip, but fails to regulate microtubule dynamics, resulting in elongated spindles, misaligned chromosomes, and unattached kinetochores. Furthermore, these data indicate that these changes lead to prematurely increased egg aneuploidy, translating finally to an accelerated decline in female fertility, suggesting an inherited genetic mechanism of female infertility via the kinesin motor domain.

Discussion

In this study, we employed a bioinformatic strategy to identify plausible common pathological variants of accelerated loss of egg quality. This report implicates kinesin motor domain variation, and kinesin variants in general, as a causal genetic mechanism in female infertility patients (51). While this manuscript was in review, a report was published identifying another variant in the human *KIF18A*

Downloaded from https://www.pnas.org by 188.129.80.218 on July 30, 2025 from IP address 188.129.80.218.

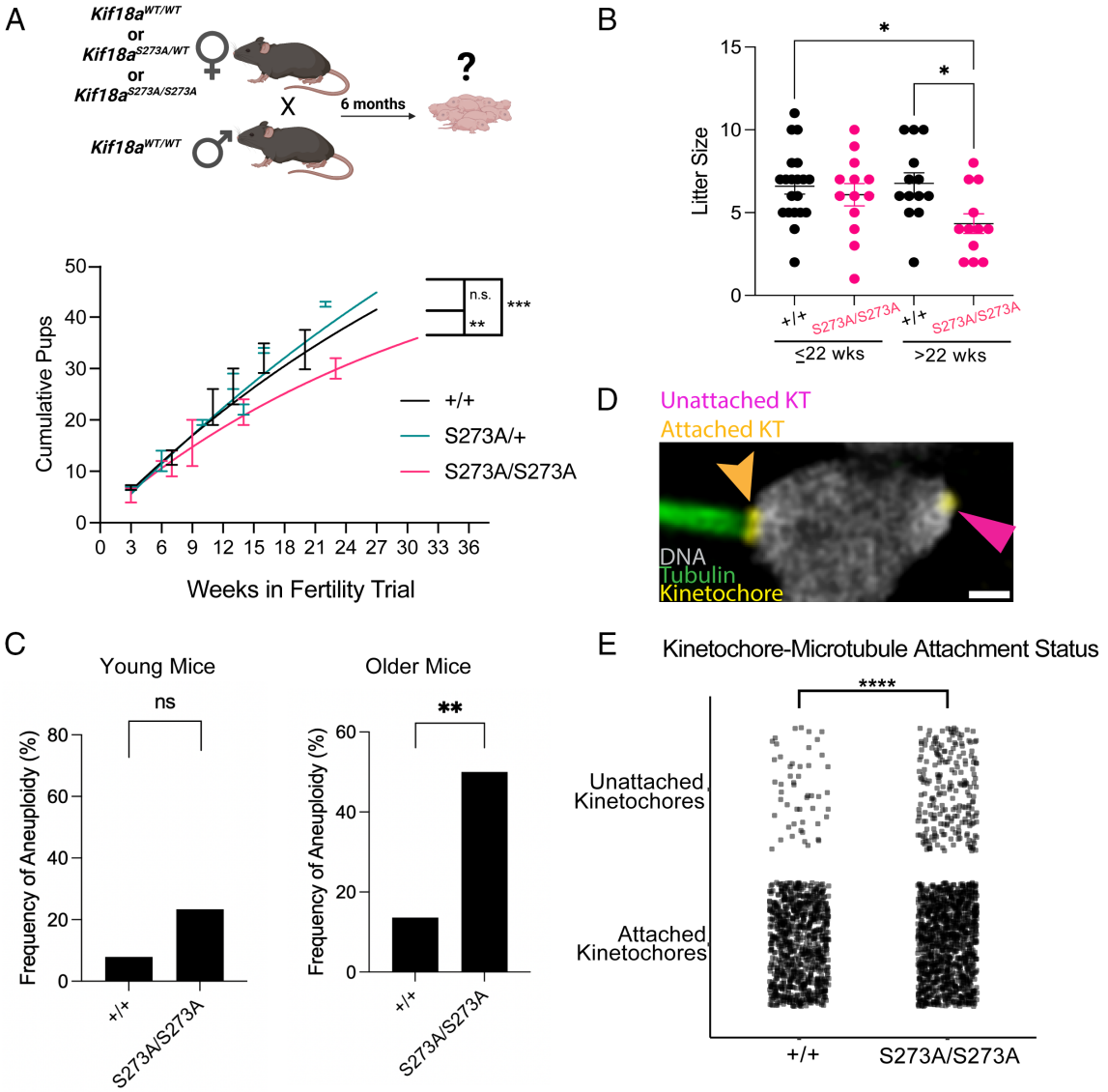

Fig. 4. Female *Kif18a*^{S273A} mice experience accelerated reproductive aging. (*A*) Cumulative pups from fertility trial. +/+ vs S273A/S273A ($P = 0.0009$). +/+, n = 5; S273A/+, n = 4; S273A/S273A, n = 4. Comparison of fits test $P = 0.0001$. Multiple comparisons: +/+ vs. S273A/+, $P = 0.706$; +/+ vs. S273A/S273A, $P = 0.0009$; S273A/+ vs. S273A/S273A, $P < 0.0001$. (*B*) Litter size analysis of young (≤22 wk) and older mice (>22 wk). ANOVA, Tukey's multiple comparisons test. $P = 0.030$; +/+ young vs. S273A/S273A older $P = 0.0371$; +/+ older vs. S273A/S273A older p = 0.0425. (*C*) Frequency of aneuploid eggs in young (8 to 10 wk) and older (>20 wk). 5 replicates. Younger: +/+, n = 38; S273A/S273A, n = 60; $P = 0.059$. Older: +/+, n = 22 oocytes; S273A/S273A, n = 30; $P = 0.008$. Data from each genotype pooled; Fisher's exact test. (*D*) Bivalent with microtubule-attached (pink arrowhead) and -unattached kinetochores (orange arrowhead). DNA (gray), alpha-tubulin (green), anti-centromere antibody (yellow). (*E*) Quantification of unattached and attached kinetochores. Dots represent single kinetochores. All kinetochores are pooled. +/+, n = 916; S273A/S273A, n = 1,370. Chi-square analysis. $P < 0.0001$. Data are mean ± SEM. ns, not significantly different; *$P < 0.05$; **$P < 0.01$; ***$P < 0.001$.

motor domain that is associated with female infertility (S126L) (52). These parallel findings affirm the requirement for KIF18A in mammalian oocytes and female fertility in humans.

Notably, we provide an in vivo, preclinical validation of a human genetic variant in a mouse model for the trait of EEA in female IVF patients. These findings regarding a key mechanism of female fertility and pregnancy loss are particularly timely, given the changing regulatory context of female fertility, the increase in maternal age at first pregnancy (from 21.4 y in 1970 to 27.3 y in 2021) (53, 54), and the rapidly expanding use of assisted reproductive technologies, resulting in 3% of all US infants (55).

Genetic variation may explain some of the heterogeneity in the relationship between egg aneuploidy and maternal age: Genetic variants have been identified in multiple genes that may influence egg and embryonic aneuploidy at younger-than-average ages (56, 57). For example, one genetic variant in *CEP120* was identified in individuals with higher-than-average aneuploidy, and its function was demonstrated in an in vitro mouse oocyte system (58). Human alleles in mismatch repair genes *MLH1* and *MLH3* identified in gnomAD and predicted to be pathogenetic caused age-dependent decreases in litter size and elevated meiotic aneuploidy when modeled in mice (59). However, to date, no aneuploidy-causing variant identified in fertility patients with EEA has been biologically validated in a whole-organism model. The organism-level validation is important because another study of oocyte meiosis genes demonstrates that in vitro perturbations may not translate to in vivo pathogenicity (60). Furthermore, no human genetic variants have yet been identified to cause EEA specifically via accelerated maternal aging, as we demonstrate here. As a result, no predictive genetic biomarkers of EEA exist. One major obstacle to the identification of EEA variants is the paucity of genotype–phenotype data available, resulting in relatively small patient cohorts. Functional biological validation of candidates thus is a "gold standard" to identify true genetic causality in EEA.

Downloaded from https://www.pnas.org by 188.129.80.218 on July 30, 2025 from IP address 188.129.80.218.

We found that kinesin motor domain variants in *KIF20A* and *KIF18A* identified in EEA patients had a deleterious effect on mouse oocytes via our overexpression bioassay, causing aneuploidy and abrogating gene-specific functions required for correct chromosome segregation (Fig. 5). When we knocked the homologous variant of KIF18A^{T273A} into the endogenous *Kif18a* locus in the mouse, we found that homozygous mutants had increased egg aneuploidy and decreased fertility at moderately advanced maternal age. T273 resides in the KIF18A motor domain, specifically in the Loop 11/Switch II region of the kinesin, and resides at the boundary of the α4 helix (61–63). The α4 helix region is implicated in tubulin binding. Phosphorylation of nearby S284 alters motor directionality causing chromosome misalignment and changes in spindle length (62). Although we do not know whether T273 is a phospho-acceptor site, our data are consistent with altered function when a residue in this critical region is altered.

A recent report asserted that KIF18A is nonessential in meiosis I based on a ZP3-Cre *Kif18a* knockout (44), a statement seemingly in conflict with the results shown here and elsewhere (52). However, the experiments shown here found an effect with age. In contrast, the ZP3-Cre *Kif18a* knockout was only evaluated in young mice. When considered in this light, our work aligns with and stretches beyond the existing literature. Homozygous mutant mice did not show subfertility until they approached ~20 wk of age, which is biologically akin to a human's late twenties and early thirties (64) and parallels the human patient data (Fig. 1*A*). Our data suggest that this variant is pathogenic for EEA only when coupled with a "second hit" of normal mechanisms of aging, revealing a complex genotype–phenotype relationship. It is well established that cohesin, the molecular "glue," is lost progressively from chromosomes in aging human and mouse oocytes, resulting in age-dependent increases in aneuploidy (6–9). We speculate that early loss of cohesin in 4-mo-old mice is insufficient to cause aneuploidy in Kif18A-WT mice, but it is sufficient to cause aneuploidy in mice homozygous for *KIF18A*^{T273A}. Other mechanisms, such as age-dependent changes in spindle assembly (65), could also interact with *KIF18A*^{T273A} in this two-hit or a multihit mechanism. Further experimental analysis would be required to elucidate the precise molecular interplay between maternal aging, KIF18A, and egg aneuploidy. Large-scale human trials are required to ultimately determine the diagnostic utility of *KIF18A*^{T273A} and other kinesin motor domain variants.

A recent GWAS (13) identified genes contributing to age at natural menopause, emphasizing the role of DNA damage response genes in the timing of menopause onset. *KIF18A* and *KIF20A* were not identified as significantly contributing to age of menopause onset. This finding aligns with our results because menopause is largely driven by a loss of follicle quantity, whereas the kinesin motor domain mutations we identified primarily impact oocyte quality by increasing egg aneuploidy. These mutations likely exert their effects through mechanisms distinct from those influencing follicle depletion, which may explain why they were not detected in the GWAS focused on menopause timing.

KIF18A^{T273A} is enriched in the high-risk fertility patient cohort, with both homozygotes and heterozygotes. Notably, the single homozygous patient, a 25-y-old, exhibited 45% aneuploidy, suggesting a more pronounced effect in the homozygous state. In our mouse model, heterozygosity for the *KIF18A*^{S273A} allele did not impact fertility, while homozygosity accelerated reproductive aging, indicating that the allele functions in a recessive manner in mice, but may have an incompletely dominant effect in humans. It is likely that this discrepancy in aneuploidy rates exists due to the more robust meiotic process that exists in mouse oocytes as compared to human oocytes; in studies of reproductively young individuals, ~5% of mouse eggs are aneuploid (9, 66, 67), and ~20% of human eggs are aneuploid (5, 68, 69).

Because KIF18A homodimerizes (70), in a heterozygous cellular context, three KIF18A dimers could exist: WT-WT dimers, WT-T273A dimers, and T273A-T273A dimers, possibly in an equal distribution. In the homozygous context, only one type of dimer is possible. Therefore, heterozygosity offers the possibilities of the mutant monomer poisoning a WT-T273A KIF18A dimer

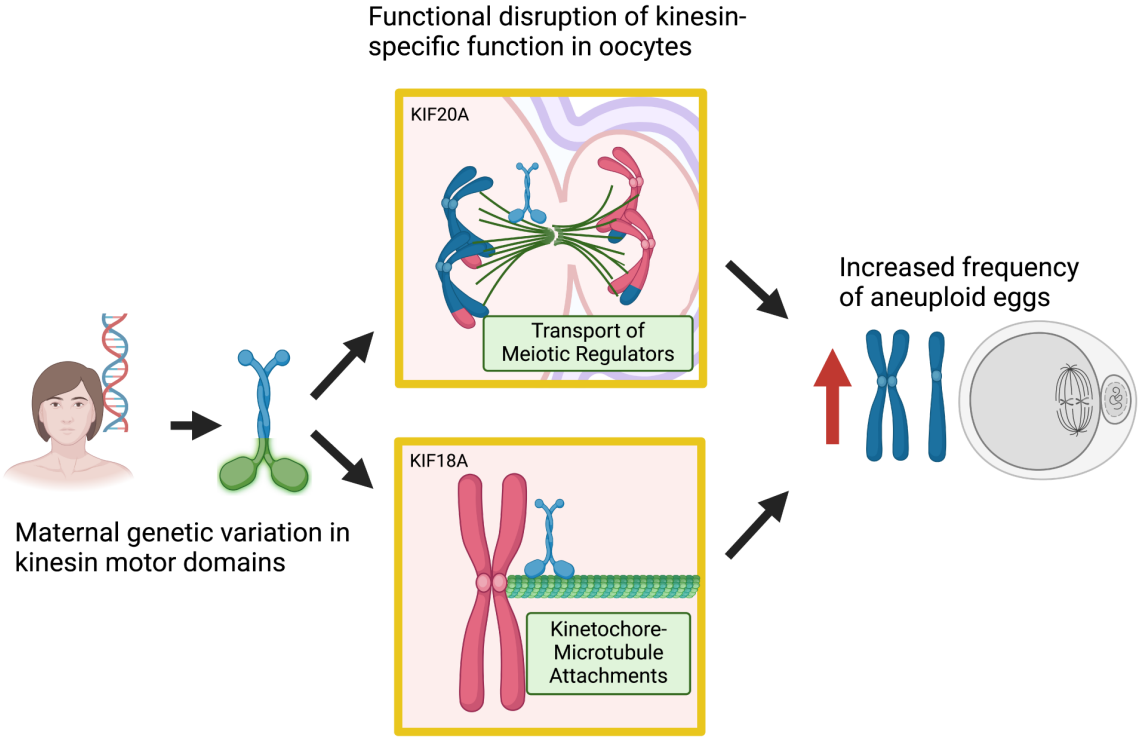

Fig. 5. Summary schematic of overall findings.

Downloaded from https://www.pnas.org by 188.129.80.218 on July 30, 2025 from IP address 188.129.80.218.

and, alternatively or additionally, of the net cellular contribution of the T273A-T273A KIF18A dimer being insufficient to support accurate chromosome segregation. In contrast, homozygosity permits only the latter. Our in vitro overexpression experiments likely more closely approximate homozygosity, in which T273A-T273A KIF18A dimers are the predominant form. These results suggest that the dosage of KIF18A^{T273A} and the meiotic context both determine the pathogenicity of the allele in terms of egg aneuploidy.

Our study has several limitations. The sample size of our patient cohort is relatively small, limiting our power to identify variants and genes contributing to the aneuploidy risk. To address this limitation, we developed an enhanced variant prioritization pipeline and performed deep biological validation, both in vitro and in vivo. However, we expect that there are other undiscovered variants that influence egg aneuploidy risk. For example, two individuals in the patient cohort both are heterozygous for the KIF18A^{T273A} variant and had no aneuploid embryos. We speculate that this is attributable to the polygenicity of the trait of egg aneuploidy, a hypothesis supported by earlier findings that some genetic variants protect against egg aneuploidy in vitro (71). Another limitation is that our analysis focuses on women with primarily European ancestry, which is due to the overrepresentation of this group in the sampled fertility clinic patient populations. Therefore, our results may not generalize to other ethnic groups. New genomic biobanks of egg aneuploidy phenotypes and future analyses of ultralow-coverage genetic data from PGT-A should aim to include other ethnic groups (72). A third limitation is the use of mouse oocytes, rather than human oocytes, to biologically validate our results. Currently, the only human oocytes available for use in US-based laboratories are those that IVF clinics have discarded due to slow or arrested cell cycle progression; these oocytes would be a highly genetically heterogenous and functionally nebulous system in which to evaluate the consequence of specific genetic variants on oocyte meiosis. Mouse oocytes undergo similar meiotic maturation steps; are genetically tractable; and environmentally controlled. Bovine oocytes also undergo meiosis in a fashion like that of human oocytes (73–75). However, given short gestation period of mice compared with that of cows (<1 mo versus ~7 mo) and the shorter reproductive lifespan of mice compared with that of cows (reproductive decline at ~6 mo versus ~10 y) (76), we elected to use the transgenic mouse system for this study of fertility and reproductive aging.

This study lays the groundwork for future identification of EEA genetic variants by demonstrating an enhanced statistical and functional genetic pipeline (Fig. 1*B*) and identifies kinesin motor domains as a functional genetic hotspot for EEA (Fig. 5). Moreover, this study provides the deepest biological validation of a candidate clinical variant for causation of EEA to date and an in vivo mouse model of an EEA patient variant, paving the way for biomarker development. Identification of precision genetic biomarkers for EEA could provide a personalized approach to fertility care, bringing a genomic medicine lens to fertility treatment.

Materials and Methods

Ethical Approval, Sample Selection, and Whole-exome Sequencing Dataset. Patient DNA samples were obtained from Reproductive Medicine Associates of New Jersey (RMANJ) DNA Bank, and the project was approved by IRB #RMA1-09-165 at Copernicus Group IRB and IRB #Pro2018000106 at Rutgers University. Preimplantation genetic testing for aneuploidy (PGT-A) was performed on biopsies of trophectoderm cells from day 5 human blastocysts. Aneuploidy rate was calculated for "White, non-Hispanic" patients with a minimum of four embryos tested. Samples with extreme aneuploidy rates were selected using a robust nonlinear regression analysis as previously described (27).

Whole-exome sequencing libraries were constructed by Novogene (Sacramento, CA) from maternal peripheral blood DNA samples using the Agilent SureSelect Human All Exon V6 kit by Agilent Technologies (Santa Clara, CA). The libraries were sequenced on the Illumina sequencing platform using the 2 × 150 base-pairs paired-end format (Illumina, San Diego, CA). Data were aligned to the human reference genome (hg19) using BWA (77), and the joint genotyping was performed using the GATK v3.8 pipeline following the GATK best practices (78). The sample and variant quality control was described in detail in the previous publication (27).

Gene Prioritization with VAAST. The Variant Annotation, Analysis and Search Tool (VAAST) (28) was applied to identify candidate genes associated with high aneuploidy risk, as previously described (58). VAAST was run with the following parameters: $ VAAST -lh y -r 0.05 -d 1e5 -o outputfile -m lrt -k ref_gff controls.cdr cases.cdr

GO and Protein–protein Interaction Network Analyses. GO enrichment analysis was performed using the overrepresentation analysis tool on CPDB (http://cpdb.molgen.mpg.de/) (79) on candidate genes with *P*-values smaller than 0.05 in the VAAST analysis. To investigate protein–protein interaction (PPI) networks among VAAST genes, three databases were used: CPDB (79), STRING (80), and GIANT_v2 (81, 82). All types of interactions from the three databases were combined and filtered for the network construction, as previously described (57, 83). The network was constructed using a customized Python code (https://github.com/JXing-Lab/network-ppi).

Modules within the PPI network were identified using PAPER (30), a program which employs the "Preferential Attachment Plus Erdős–Rényi" model for community detection within a network. PAPER was run on the original PPI network using the following parameters: method = collapsed; Burn = 1000; M = 5000; size_thresh = 0.02; birth_thresh = 0.6. EMP (https://github.com/Shamir-Lab/EMP) was used to conduct the GO enrichment analysis on each discovered module and to calculate its empirical *P*-value (84).

Validation of the Variants. Seven candidate variants in *KIF18A and KIF20A* were PCR amplified, and the amplicons were sequenced using Illumina Nextseq (San Diego, CA) at the Foundation for Embryonic Competence (*SI Appendix*, Table S6). All variants except one (*KIF20A:* chr5:137522092_C_T in hg19 coordinates) were validated. Therefore, *KIF20A:* chr5:137522092_C_T was excluded from the analyses.

Mice. Sexually mature CF-1 female mice [6 to 10 wk of age, Envigo (Indianapolis, IN)] were used in this study, with the exception of the *Kif18a* knock-in mice. For *Kif18a* knock-in mice, *Kif18a* variant alleles were generated using CRISPR-Cas9 genome editing through Rutgers Genome Editing Shared Resource (New Brunswick, NJ). C57BL/6 J zygotes were microinjected with a mixture containing Cas9 protein (IDT, San Diego, CA), an sgRNA (MilliporeSigma, Burlington, MA), and an ssODN (IDT, San Diego, CA), which contained homology arms and the S273A mutation (*SI Appendix*, Table S7). Ear biopsies from founders were screened by PCR at the mutation site and the PCR products were digested with restriction enzyme *Hha I* (introduced by S273A and PAM change) to select founders with the homologous S273A change. PCR products from the selected founders were then subjected to next-generation sequencing using the Amplicon EZ kit by Azenta Life Sciences (Burlington, MA) to confirm the S273A change. Homozygous founder mice (F0) were confirmed using Sanger sequencing. Founders were backcrossed to C57B6/J mice from Jackson Laboratory (Bar Harbor, ME) for two generations, and progeny were screened using PCR primers *KIF18AA* and *KIF18AB* (*SI Appendix*, Table S7) by the gain of *Hha* I restriction site or by Sanger sequencing of PCR products. Then, animals were maintained in a C57B6/J background.

Housing and breeding use a 12 h light/12 h dark cycle, and constant temperature was performed in the animal facility at Rutgers, the State University of New Jersey. Food and water were provided ad libitum. All animal experiments performed in this study were approved by the Rutgers IACUC (protocol #201702497) and followed the guidelines set by the NIH.

Oocyte Collection and In Vitro Maturation. Prophase I oocytes were collected as described (85) in minimum essential medium (MEM; #M0268, MilliporeSigma, Burlington, MA) containing 2.5 μM milrinone (#M4659, MilliporeSigma, Burlington, MA) to prevent the spontaneous meiotic resumption (86). Briefly, two days before oocyte collection, mice were primed with pregnant mare serum gonadotropin (PMSG, #493-10, Lee Biosolutions, Maryland Heights,

Downloaded from https://www.pnas.org by 188.129.80.218 on July 30, 2025 from IP address 188.129.80.218.

MO). After collection in MEM, oocytes were incubated in Chatot, Ziomek, and Bavister (CZB) medium (87) without milrinone, in 5% CO_2 and 37 °C for the desired time of maturation depending on the meiotic stages to be evaluated (7 h for Metaphase I, 10 h for Telophase I, and 16 h for Metaphase II).

Drug Treatments. Oocytes were cultured in CZB medium treated with DMSO (control), 15 μM Paprotrain (#512533, Millipore-Sigma, Burlington, MA), or 500 nM Sovilnesib (#TA9H98DB1F0F, Millipore-Sigma, Burlington, MA). To assess maturation kinetics, oocytes were cultured in CZB after milrinone washout while in an EVOS M7000 Imaging System (Invitrogen, # AMF7000) at 37 °C with 5% CO_2. Oocytes were scored visually for nuclear envelope breakdown and polar body extrusion (PBE) as a proxy for metaphase II. To assess AURKC migration at Telophase I, oocytes were matured in CZB with the indicated dose of Paprotrain for 10 h (0 μM) or 14 h (15 μM) to adjust for the drug-dependent delay in maturation timing. To assess aneuploidy in oocytes treated with either Paprotrain or Sovilnesib, oocytes were matured in CZB with the indicated doses for 16 h. Subsequently, aneuploidy was assessed as described in the "in situ chromosome counting" section.

Constructs and cRNA Generation. To generate cRNA of *KIF20A* and *KIF18A* fused with enhanced green fluorescent protein (eGFP), the full-length coding sequences (CDS) of genes encoding human *KIF20A* (NM_005733.3) and *KIF18A* (NM_031217.4) were amplified from clones OHu24388 (GenScript, Piscataway, NJ) and OHu28001D (GenScript, Piscatway, NJ), respectively. The amplified CDSs were ligated into the in vitro transcription (pIVT) vector (88) containing eGFP fusion using the following primers:

KIF20A; For: 5′-ATGCGTCGACATGTCGCAAGGGATCCTTTCTC-3′, Rev: 5′-GGGCG TCTAGAGTACTTTTTGCCAAAAGGCC-3′

KIF18A; For: 5′-ATGCGTCGACATGTCTGTCACTGAGGAAGACCTG-3′, Rev: 5′-GC GGCGTCTAGATCTTAGATTTCCTTTTG-3′. All inserts were sequenced fully to ensure no PCR-induced mutations were introduced.

Mutagenesis was performed using the multisite-directed mutagenesis kit (#210515, Agilent Technologies, Santa Clara, CA) according to the manufacturer's instructions. To mimic the human variants, pIVT-*KIF20A-GFP-WT* and *KIF18A-GFP-WT* plasmids were mutated using the following primers that contain the same variant nucleotide substitutions (in bold and underlined)

Motor domain kinesin variants. Kif20A p.Leu191Pro: 5′-GCTGATCTTCAATAGC C**C**CCAAGGCCAACTTCATC-3′

Kif20A p.Asn483Ser: 5′-AGGCCGTTCCTGCATGATTGTCA**G**TGTGAATCCCTG-3′ Kif18A p.Thr273Ala: 5′-TCCGGTGCTAAGGGGG**C**CCGATTTGTA**G**AAG-3′

Nonmotor domain kinesin variants (related to SI Appendix, Fig. S3). Kif20A p.Ser44Phe: 5′-CCTGCTATCAGACTGC**T**TTGTCGTCTCTACCTC-3′

Kif20A p.Glu63Lys: 5′-TCCATCTGAG**G**GACAGTATG**A**AGAAGGTGAAAGTATACTTG-3′

Kif18A p.Ser835Arg: 5′-AAAAGGAAACGGAAA**T**TAACAAG**G**TCTACATCAAACAGT TCGTTAAC-3′

Mutations were confirmed by Sanger sequencing (Azenta, Piscataway, NJ). *Kif20A* plasmids were linearized with *Ssp I* (#R0132S, New England Biolabs, Ipswich, MA) and *Kif18A* plasmids with *Kas I* (#R0544S, New England Biolabs, Ipswich, MA) restriction enzymes. pGEMHE-mEGFP-mTrim21 (#105519, Addgene, Watertown, MA) plasmid was linearized with AscI (#R0558S, New England Biolabs, Ipswich, MA). All linearized plasmids were then purified with the QIAquick PCR Purification kit (#28104, Qiagen, Venlo, The Netherlands) and in vitro transcribed using a T7 mMessage mMachine Kit (#AM1345, Thermo Fisher Scientific, Waltham, MA). The cRNAs were purified using an RNAeasy kit (#74104, Qiagen, Venlo, The Netherlands) and stored at −80 °C.

Microinjection. Prophase I-arrested oocytes were microinjected with the indicated cRNAs in MEM containing milrinone using a Xenoworks microinjector (Sutter Instruments, Novato, CA) as described before (89). Then, oocytes were kept in milrinone-containing CZB medium for at least 2 h or overnight for protein expression before downstream assays.

In Situ Chromosome Counting. As described previously (90), after in vitro maturation of Prophase I oocytes for 16 h, Metaphase II eggs were incubated with 100 μM Monastrol (#M8515, MilliporeSigma, Burlington, MA), dissolved in dimethyl sulfoxide (#472301, MilliporeSigma, Burlington, MA) in CZB medium for 2 h before fixation in 2% paraformaldehyde (PFA, #P6148, MilliporeSigma, Burlington, MA) in phosphate-buffered saline (PBS). Eggs were stained with Anti-Centromeric Antibody (IF: 1:30; #15-234, Antibodies Incorporated, Davis, CA) to detect centromeres and mounted in VectaShield (#H-1000, Vector Laboratories, Newark, CA) with 4′,6-Diamidino-2-Phenylindole, Dihydrochloride (DAPI; #D1306; 1:170, Life Technologies, Carlsbad, CA). Eggs were imaged using a Leica SP8 confocal with 0.5-μm z-intervals. Chromosome counting was performed with NIH ImageJ software (91). The normal chromosome number for a mouse egg is 20 pairs of sister chromatids; an egg with any deviation from this number was considered aneuploid.

Female Fertility Trials. Sexually mature female mice (8 to 10 wk old) bearing *Kif18a*$^{+/+}$, *Kif18a*$^{S273A/+}$, or *Kif18a*$^{S273A/S273A}$ genotypes were housed in monogamous pairings with B6D2F1/J male mice (Jackson Laboratory, Bar Harbor, ME). The animals remained paired for six months and were allowed to breed freely. Daily observations were made for pup counting starting at day 18 based on the mouse gestational period (18-21 d).

Histology. Subsequent to each fertility trial, female mice harboring the *KIF18A* alleles were euthanized according to the approved procedure by the Rutgers University Institutional Animal Care and Use Committee (IACUC), and ovaries were collected for histology. Ovaries were fixed in Davidson's modified fixative (overnight at 4 °C), washed in 70% ethanol, embedded in paraffin, serially sectioned (5 μm), and stained with hematoxylin and eosin (H&E) (Rutgers Translational Sciences Research Pathology Services, Piscataway, NJ). Three ovarian sections per animal were evaluated for the presence of *corpora lutea* to confirm ovulation.

Antibodies for Oocyte Immunofluorescence and Western Blotting. The following primary antibodies were used for immunofluorescence (IF) and western blotting (WB): rabbit anti-KIF18A (IF:1:50, #19245-1-AP, ProteinTech, Rosemont, IL), mouse anti-KIF20A (IF:1:100, #67190-1-Ig, ProteinTech, Rosemont, IL), rabbit anti-GFP (WB:1:500, #G1544, MilliporeSigma, Burlington, MA), rabbit anti-α-tubulin (WB: 1:1,000; IF:1;50; #11H10, Cell Signaling Technology, Danvers, MA), sheep anti-alpha/beta-tubulin (IF:1:100, #ATN02, Cytoskeleton, Denver, CO), Rabbit anti-EEA1 (IF:1:100, #3288 T, Cell Signaling Technology, Danvers, MA), human ACA (IF: 1:30; #15-234, Antibodies Incorporated, Davis, CA), rabbit anti-AURKC (IF: 1:200; #A400-023A-BL1217, Bethyl Laboratories, Montgomery, TX), mouse anti-acetylated α-tubulin (IF: 1:100, #T7451, MilliporeSigma, Burlington, MA), and IgG antibody (trim away:0.5 mg/ml, #12-371, MilliporeSigma, Burlington, MA). Goat anti-human-Alexa-633 (IF: 1:200; #A21091, Life Technologies, Carlsbad, CA) and donkey anti-rabbit-Alexa-568 (IF: 1:200; #A10042, Life Technologies, Carlsbad, CA), anti-alpha/beta-tubulin (IF: 1:100, #ATN02, Cytoskeleton, Denver, CO), and anti-HRB (WB: 1:1000; rabbit, #R1006, Kindle Biosciences, Greenwich, CT) were used as secondary antibodies.

Immunofluorescence was performed as described previously (85). Briefly, the oocytes were fixed in 2% PFA at room temperature for 20 min. Blocking buffer (0.3% BSA in PBS with 0.01% Tween-20) was used to wash out the fixative solution three times for 10 min. Oocytes were then permeabilized in PBS containing 0.2% Triton-X-100 for 20 min and blocked in blocking buffer for 10 min. Primary antibody incubation was performed for 1 h at room temperature in a dark, humidified chamber, followed by three washes of 10 min each in blocking solution. Then, oocytes were incubated in secondary antibody for 1 h in a dark humidified chamber, followed by three washes of 10 min each in blocking buffer. Finally, oocytes were mounted in 10 μl of VectaShield with DAPI.

Oocyte Microscopy and Image Analysis. Images were acquired using a Leica TCS SP8 confocal microscope equipped with a 63× objective, 1.40 N.A. oil immersion objective. For each image, optical z-slices were obtained using a 0.5 to 1 μm step length with a zoom setting of 2.5 to 4. Laser powers were kept constant for pixel intensity comparisons. Images were analyzed using NIH ImageJ software (91) or Imaris 9.9.1 from Bitplane (Zürich, Switzerland).

AURKC Localization Analysis. Images of immunolabeled telophase oocytes were analyzed with Imaris 9.9.1. In Imaris, a line plot was constructed across the midzone spindle and the signal intensity representing AURKC was measured. Z-slices from each image were merged into a projection.

Kinetochore–microtubule Attachment Assay. Oocytes matured for 8 h (Metaphase I) were transiently exposed to cold temperatures to depolymerize microtubules unattached to kinetochores. Oocytes were then immediately fixed in 2% PFA at room temperature for 20 min and blocked overnight. Oocytes were

Downloaded from https://www.pnas.org by 188.129.80.218 on July 30, 2025 from IP address 188.129.80.218.

probed for alpha-tubulin and CREST and counterstained with DAPI. Oocytes were imaged using the protocol described above with the addition of Leica SP8 Lightning deconvolution. Images of immunolabeled cold-treated Metaphase I oocytes were analyzed in Imaris 10.1.1. Kinetochore foci were masked using the "spots" tool in Imaris. For each experiment, the median intensity of tubulin signal per kinetochore focus was used to determine whether each kinetochore overlapped with a microtubule bundle. Intensity thresholds were manually verified using at least 50+ kinetochores across 5 + oocytes per imaging set to account for interexperimental variation.

Variant Stability Prediction Modeling. Variants were modeled for their effect on protein stability in terms of ΔΔG. Previously solved protein structures were obtained from the RSCB Protein DataBank (www.rscb.org) (92). For KIF20A, Accession Number 8F1A was used (93). For KIF18A, Accession Number 5OGC was used (94). Each structure was inputted into the PoPMuSiC tool (www.dezyme.org) (38), and the human variant information was inputted to generate a ΔΔG prediction.

Statistical Analysis. Unpaired Student's *t* test and one-way ANOVA based on the group numbers were used to evaluate the differences between groups using GraphPad Prism. The differences with $P < 0.05$ were considered significant. The error bars indicate the SEM. For the chromosome counting analysis of knock-in mice, oocyte data were pooled and analyzed as contingency outcomes via two-sided Fisher's exact test. Female fertility was modeled using nonlinear regression with an exponential plateau model. The similarity of the fertility between genotypes was evaluated using the extra sum-of-squares F test. Multiple comparison corrections were performed using Tukey's multiple comparison test. For both male and female trials, no outliers were identified as determined by Robust regression and Outlier removal (ROUT) analysis performed for each genotype at a Q coefficient of 1%.

Data, Materials, and Software Availability. The variants identified in this study, along with their allele frequencies in sequenced samples, are available at Rutgers University Community Repository (RUcore) (95).

ACKNOWLEDGMENTS. We thank members of the Schindler and Xing labs for their helpful comments, Warif El Yakoubi for the preliminary Paprotrain studies, and Erin Mallory for assistance with histology slides. This work was supported by NIH grant R01HD091331 to K.S. and J.X. L.B. is supported by NIH fellowship F30HD107976 and the Foundation for Women's Wellness. L.B. was supported by NIH grant T32GM139804. The Tolić lab is funded by the European Research Council (ERC Synergy Grant, GA Number 855158), the Croatian Science Foundation (HRZZ) through Swiss-Croatian Bilateral Projects (project IPCH-2022-10-9344), and projects cofinanced by the Croatian Government and the European Union through the European Regional Development Fund–the Competitiveness and Cohesion Operational Programme: IPSted (Grant KK.01.1.1.04.0057) and QuantiXLie Center of Excellence (Grant KK.01.1.1.01.0004).

Author affiliations: [a]Department of Genetics, Rutgers, The State University of New Jersey, Piscataway, NJ 08854; [b]Human Genetics Institute of New Jersey, Rutgers, The State University of New Jersey, Piscataway, NJ 08854; [c]Rutgers Robert Wood Johnson Medical School, Rutgers, The State University of New Jersey, Piscataway, NJ 08854; [d]Department of Theriogenology, Faculty of Veterinary Medicine, Mansoura University, Mansoura 35516, Egypt; [e]Department of Molecular Biology, Ruđer Bošković Institute, Zagreb 1000, Croatia; [f]Juno Genetics US, Basking Ridge, NJ 07920; [g]Department of Statistics, Rutgers, The State University of New Jersey, Piscataway, NJ 08854; and [h]Foundation for Embryonic Competence, Basking Ridge, NJ 07920

1. S. A. Yatsenko, A. Rajkovic, Genetics of human female infertilitydagger. *Biol. Reprod.* **101**, 549–566 (2019).
2. J. Wu *et al.*, IDDB: A comprehensive resource featuring genes, variants and characteristics associated with infertility. *Nucleic Acids Res.* **49**, D1218–D1224 (2021).
3. T. Hassold, H. Hall, P. Hunt, The origin of human aneuploidy: Where we have been, where we are going. *Hum. Mol. Genet.* **16**, R203–208 (2007).
4. S. I. Nagaoka, T. J. Hassold, P. A. Hunt, Human aneuploidy: Mechanisms and new insights into an age-old problem. *Nat. Rev. Genet.* **13**, 493–504 (2012).
5. T. Hassold, P. Hunt, To err (meiotically) is human: The genesis of human aneuploidy. *Nat. Rev. Genet.* **2**, 280–291 (2001).
6. B. P. Mihalas *et al.*, Age-dependent loss of cohesion protection in human oocytes. *Curr. Biol.* **34**, 117–131.e15 (2024).
7. F. E. Duncan *et al.*, Chromosome cohesion decreases in human eggs with advanced maternal age. *Aging Cell* **11**, 1121–1124 (2012).
8. T. Chiang, R. M. Schultz, M. A. Lampson, Meiotic origins of maternal age-related aneuploidy. *Biol. Reprod.* **86**, 1–7 (2012).
9. T. Chiang, F. E. Duncan, K. Schindler, R. M. Schultz, M. A. Lampson, Evidence that weakened centromere cohesion is a leading cause of age-related aneuploidy in oocytes. *Curr. Biol.* **20**, 1522–1528 (2010).
10. O. American College of, P. Gynecologists Committee on Gynecologic, C. Practice, Female age-related fertility decline. Committee Opinion No. 589. *Fertil. Steril.* **101**, 633–634 (2014).
11. J. Menken, J. Trussell, U. Larsen, Age and infertility. *Science* **233**, 1389–1394 (1986).
12. L. Biswas *et al.*, Meiosis interrupted: The genetics of female infertility via meiotic failure. *Reproduction* **161**, R13–R35 (2021).
13. K. S. Ruth *et al.*, Genetic insights into biological mechanisms governing human ovarian ageing. *Nature* **596**, 393–397 (2021).
14. K. M. Tyc, R. C. McCoy, K. Schindler, J. Xing, Mathematical modeling of human oocyte aneuploidy. *Proc. Natl. Acad. Sci. U.S.A.* **117**, 10455–10464 (2020).
15. S. A. Endow, F. J. Kull, H. Liu, Kinesins at a glance. *J. Cell Sci.* **123**, 3420–3424 (2010).
16. F. J. Kull, E. P. Sablin, R. Lau, R. J. Fletterick, R. D. Vale, Crystal structure of the kinesin motor domain reveals a structural similarity to myosin. *Nature* **380**, 550–555 (1996).
17. S. Gilbert, S. Sardar, "4.17 Kinesin Structure and Biochemistry" in *Comprehensive Biophysics*, E. H. Egelman, Ed. (Academic Press, 2012), **vol. 4**, pp. 321–344.
18. A. Echard *et al.*, Interaction of a Golgi-associated kinesin-like protein with Rab6. *Science* **279**, 580–585 (1998).
19. I. E. Adriaans *et al.*, MKLP2 is a motile kinesin that transports the chromosomal passenger complex during anaphase. *Curr. Biol.* **30**, 2628–2637.e29 (2020).
20. K. J. Verhey, J. W. Hammond, Traffic control: Regulation of kinesin motors. *Nat. Rev. Mol. Cell Biol.* **10**, 765–777 (2009).
21. Z. Jin *et al.*, Expression, regulating mechanism and therapeutic target of KIF20A in multiple cancer. *Heliyon* **9**, e13195 (2023).
22. M. Serena, R. N. Bastos, P. R. Elliott, F. A. Barr, Molecular basis of MKLP2-dependent Aurora B transport from chromatin to the anaphase central spindle. *J. Cell Biol.* **219**, e201910059 (2020).
23. B. Orr *et al.*, An anaphase surveillance mechanism prevents micronuclei formation from frequent chromosome segregation errors. *Cell Rep.* **37**, 109783 (2021).
24. J. Stumpff, M. Wagenbach, A. Franck, C. L. Asbury, L. Wordeman, Kif18A and chromokinesins confine centromere movements via microtubule growth suppression and spatial control of kinetochore tension. *Dev. Cell* **22**, 1017–1029 (2012).
25. J. Stumpff, G. von Dassow, M. Wagenbach, C. Asbury, L. Wordeman, The kinesin-8 motor Kif18A suppresses kinetochore movements to control mitotic chromosome alignment. *Dev Cell* **14**, 252–262 (2008).
26. Y. Cohen-Sharir *et al.*, Aneuploidy renders cancer cells vulnerable to mitotic checkpoint inhibition. *Nature* **590**, 486–491 (2021).
27. K. M. Tyc *et al.*, Analysis of DNA variants in miRNAs and miRNA 3′UTR binding sites in female infertility patients. *Lab. Invest.* **101**, 503–512 (2020). 10.1038/s41374-020-00498-x.
28. H. Hu *et al.*, VAAST 2.0: Improved variant classification and disease-gene identification using a conservation-controlled amino acid substitution matrix. *Genet. Epidemiol.* **37**, 622–634 (2013).
29. H. Motenko, S. B. Neuhauser, M. O'Keefe, J. E. Richardson, MouseMine: A new data warehouse for MGI. *Mamm. Genome.* **26**, 325–330 (2015).
30. H. Crane, M. Xu, Root and community inference on the latent growth process of a network. arXiv [Preprint] (2023). https://doi.org/10.48550/arXiv.2107.00153 (Accessed 15 October 2024).
31. J. Liu *et al.*, MKlp2 inhibitor paprotrain affects polar body extrusion during mouse oocyte maturation. *Reprod. Biol. Endocrinol.* **11**, 117 (2013).
32. Y. Zhang *et al.*, KIF20A regulates porcine oocyte maturation and early embryo development. *PLoS One* **9**, e102898 (2014).
33. M. I. Mayr *et al.*, The human kinesin Kif18A is a motile microtubule depolymerase essential for chromosome congression. *Curr. Biol.* **17**, 488–498 (2007).
34. F. Tang *et al.*, Kif18a regulates Sirt2-mediated tubulin acetylation for spindle organization during mouse oocyte meiosis. *Cell Div.* **13**, 9 (2018).
35. M. M. Möckel, A. Heim, T. Tischer, T. U. Mayer, Xenopus laevis Kif18A is a highly processive kinesin required for meiotic spindle integrity. *Biol. Open* **6**, 463–470 (2017).
36. I. Amgen, KIF18A Inhibitors for Treatment of Neoplastic Diseases. W. I. P. Organization, ed. (2021).
37. C. Labriere *et al.*, New MKLP-2 inhibitors in the paprotrain series: Design, synthesis and biological evaluations. *Bioorg. Med. Chem.* **24**, 721–734 (2016).
38. F. Pucci, K. V. Bernaerts, J. M. Kwasigroch, M. Rooman, Quantification of biases in predictions of protein stability changes upon mutations. *Bioinformatics* **34**, 3659–3665 (2018).
39. U. Gruneberg, R. Neef, R. Honda, E. A. Nigg, F. A. Barr, Relocation of Aurora B from centromeres to the central spindle at the metaphase to anaphase transition requires MKlp2. *J. Cell Biol.* **166**, 167–172 (2004).
40. G. I. Jung *et al.*, An oocyte meiotic midbody cap is required for developmental competence in mice. *Nat. Commun.* **14**, 7419 (2023).
41. K. T. Yang *et al.*, Aurora-C kinase deficiency causes cytokinesis failure in meiosis I and production of large polyploid oocytes in mice. *Mol. Biol. Cell* **21**, 2371–2383 (2010).
42. A. L. Nguyen *et al.*, Genetic Interactions between the Aurora Kinases Reveal New Requirements for AURKB and AURKC during Oocyte Meiosis. *Curr. Biol.* **28**, 3458–3468.e55 (2018).
43. Y. Du, C. A. English, R. Ohi, The kinesin-8 Kif18A dampens microtubule plus-end dynamics. *Curr. Biol.* **20**, 374–380 (2010).
44. A. I. Mihajlovic, C. Byers, L. Reinholdt, G. FitzHarris, Spindle assembly checkpoint insensitivity allows meiosis-II despite chromosomal defects in aged eggs. *EMBO Rep.* **24**, e57227 (2023).
45. R. Gandhi *et al.*, The Drosophila kinesin-like protein KLP67A is essential for mitotic and male meiotic spindle assembly. *Mol. Biol. Cell* **15**, 121–131 (2004).
46. S. C. Sun, N. H. Kim, Spindle assembly checkpoint and its regulators in meiosis. *Hum. Reprod. Update* **18**, 60–72 (2012).
47. D. N. Millband, L. Campbell, K. G. Hardwick, The awesome power of multiple model systems: Interpreting the complex nature of spindle checkpoint signaling. *Trends Cell Biol.* **12**, 205–209 (2002).

Downloaded from https://www.pnas.org by 188.129.80.218 on July 30, 2025 from IP address 188.129.80.218.

48. K. Wassmann, R. Benezra, Mitotic checkpoints: From yeast to cancer. *Curr. Opin. Genet. Dev.* **11**, 83–90 (2001).
49. L. G. Reinholdt, R. J. Munroe, S. Kamdar, J. C. Schimenti, The mouse gcd2 mutation causes primordial germ cell depletion. *Mech. Dev.* **123**, 559–569 (2006).
50. J. D. Biggers, R. B. Gwatkin, R. L. Brinster, Development of mouse embryos in organ cultures of fallopian tubes on a chemically defined medium. *Nature* **194**, 747–749 (1962).
51. L. Biswas *et al.*, Maternal genetic variants in kinesin motor domains prematurely increase egg aneuploidy. medRxiv [Preprint] (2024), 10.1101/2024.07.04.24309950 (Accessed 15 October 2024).
52. T. Wu *et al.*, Mechanisms of minor pole-mediated spindle bipolarization in human oocytes. *Science* **385**, eado1022 (2024).
53. T. J. Mathews, B. E. Hamilton, Mean Age of Mother, 1970–2000. (Centers for Disease Control, 2002).
54. S. M. J. K. Osterman, *et al.*, Births: Final Data for 2022. (Centers for Disease Control, 2022).
55. P. Saswati Sunderam *et al.*, State-Specific Assisted Reproductive Technology Surveillance, United States: 2021 Data Brief. (Centers for Disease Control, 2023).
56. L. Wartosch *et al.*, Origins and mechanisms leading to aneuploidy in human eggs. *Prenat. Diagn.* **41**, 620–630 (2021).
57. S. Sun *et al.*, Predicting embryonic aneuploidy rate in IVF patients using whole-exome sequencing. *Hum. Genet.* **141**, 1615–1627 (2022).
58. K. M. Tyc *et al.*, Exome sequencing links CEP120 mutation to maternally derived aneuploid conception risk. *Hum. Reprod.* **35**, 2134–2148 (2020).
59. P. Singh *et al.*, Human MLH1/3 variants causing aneuploidy, pregnancy loss, and premature reproductive aging. *Nat. Commun.* **12**, 5005 (2021).
60. X. Ding *et al.*, In vivo versus in silico assessment of potentially pathogenic missense variants in human reproductive genes. *Proc. Natl. Acad. Sci. U.S.A.* **120**, e2219925120. (2023).
61. C. R. Gliech *et al.*, Weakened APC/C activity at mitotic exit drives cancer vulnerability to KIF18A inhibition. *EMBO J.* **43**, 666–694 (2024).
62. K. L. Schutt *et al.*, Identification of the KIF18A alpha-4 helix as a therapeutic target for chromosomally unstable tumor cells. *Front. Mol. Biosci.* **11**, 1328077 (2024).
63. J. Atherton *et al.*, The mechanism of kinesin inhibition by kinesin-binding protein. *Elife* **9**, e61481 (2020).
64. J.G. Fox *et al.*, The Mouse in Biomedical Research (Academic Press, 2nd ed., 2007).
65. A. P. Zielinska *et al.*, Meiotic kinetochores fragment into multiple lobes upon cohesin loss in aging eggs. *Curr. Biol.* **29**, 3749–3765.e47 (2019).
66. K. T. Jones, S. I. Lane, Molecular causes of aneuploidy in mammalian eggs. *Development* **140**, 3719–3730 (2013).
67. H. Pan, P. Ma, W. Zhu, R. M. Schultz, Age-associated increase in aneuploidy and changes in gene expression in mouse eggs. *Dev. Biol.* **316**, 397–407 (2008).
68. J. R. Gruhn, E. R. Hoffmann, Errors of the egg: The establishment and progression of human aneuploidy research in the maternal germline. *Annu. Rev. Genet.* **56**, 369–390 (2022).
69. J. R. Gruhn *et al.*, Chromosome errors in human eggs shape natural fertility over reproductive life span. *Science* **365**, 1466–1469 (2019).
70. Y. Lin, Y. L. Wei, Z. Y. She, Kinesin-8 motors: Regulation of microtubule dynamics and chromosome movements. *Chromosoma* **129**, 99–110 (2020).
71. A. L. Nguyen *et al.*, Identification and characterization of Aurora kinase B and C variants associated with maternal aneuploidy. *Mol. Hum. Reprod.* **23**, 406–416 (2017).
72. S. Sun *et al.*, Identifying risk variants for embryo aneuploidy using ultra-low coverage whole-genome sequencing from preimplantation genetic testing. *Am. J. Hum. Genet.* **110**, 2092–2102 (2023).
73. M. Mahdipour *et al.*, TACC3 is important for correct progression of meiosis in bovine oocytes. *PLoS One* **10**, e0132591 (2015).
74. T. Fair, S. C. Hulshof, P. Hyttel, T. Greve, M. Boland, Oocyte ultrastructure in bovine primordial to early tertiary follicles. *Anat. Embryol (Berl)* **195**, 327–336 (1997).
75. J. J. Ireland, M. Mihm, E. Austin, M. G. Diskin, J. F. Roche, Historical perspective of turnover of dominant follicles during the bovine estrous cycle: Key concepts, studies, advancements, and terms. *J. Dairy Sci.* **83**, 1648–1658 (2000).
76. H. Iwata, Age-associated events in bovine oocytes and possible countermeasures. *Reprod. Med. Biol.* **15**, 155–164 (2016).
77. H. Li, R. Durbin, Fast and accurate short read alignment with Burrows-Wheeler transform. *Bioinformatics* **25**, 1754–1760 (2009).
78. M. A. DePristo *et al.*, A framework for variation discovery and genotyping using next-generation DNA sequencing data. *Nat. Genet.* **43**, 491–498 (2011).
79. R. Herwig, C. Hardt, M. Lienhard, A. Kamburov, Analyzing and interpreting genome data at the network level with ConsensusPathDB. *Nat. Protoc.* **11**, 1889–1907 (2016).
80. D. Szklarczyk *et al.*, The STRING database in 2017: Quality-controlled protein-protein association networks, made broadly accessible. *Nucleic Acids Res.* **45**, D362–D368 (2017).
81. C. S. Greene *et al.*, Understanding multicellular function and disease with human tissue-specific networks. *Nat. Genet.* **47**, 569–576 (2015).
82. A. K. WongA. KrishnanO. G. Troyanskaya, GIANT 2.0: Genome-scale integrated analysis of gene networks in tissues. *Nucleic Acids Res.* **46**, W65–W70 (2018).
83. X. Cao *et al.*, Whole-exome sequencing identifies genes associated with Tourette's disorder in multiplex families. *Mol. Psychiatry* **26**, 6937–6951 (2021). 10.1038/s41380-021-01094-1.
84. H. Levi, R. Elkon, R. Shamir, DOMINO: A network-based active module identification algorithm with reduced rate of false calls. *Mol. Syst. Biol.* **17**, e9593 (2021).
85. C. S. Blengini, K. Schindler, Immunofluorescence technique to detect subcellular structures critical to oocyte maturation. *Methods Mol. Biol.* **1818**, 67–76 (2018).
86. A. Tsafriri, S. Y. Chun, R. Zhang, A. J. Hsueh, M. Conti, Oocyte maturation involves compartmentalization and opposing changes of cAMP levels in follicular somatic and germ cells: Studies using selective phosphodiesterase inhibitors. *Dev. Biol.* **178**, 393–402 (1996).
87. C. L. Chatot, C. A. Ziomek, B. D. Bavister, J. L. Lewis, I. Torres, An improved culture medium supports development of random-bred 1-cell mouse embryos in vitro. *Reproduction* **86**, 679–688 (1989).
88. H. Igarashi, J. G. Knott, R. M. Schultz, C. J. Williams, Alterations of PLCbeta1 in mouse eggs change calcium oscillatory behavior following fertilization. *Dev. Biol.* **312**, 321–330 (2007).
89. P. Stein, K. Schindler, Mouse oocyte microinjection, maturation and ploidy assessment. *J. Vis. Exp.* **53**, 2851 (2011). 10.3791/2851.
90. C. S. Blengini, A. L. Nguyen, M. Aboelenain, K. Schindler, Age-dependent integrity of the meiotic spindle assembly checkpoint in females requires Aurora kinase B. *Aging Cell* **20**, e13489 (2021).
91. C. A. Schneider, W. S. Rasband, K. W. Eliceiri, NIH Image to ImageJ: 25 years of image analysis. *Nat. Methods* **9**, 671–675 (2012).
92. H. M. Berman *et al.*, The protein data bank. *Nucleic Acids Res.* **28**, 235–242 (2000).
93. F. M. Ranaivoson *et al.*, Nucleotide-free structures of KIF20A illuminate atypical mechanochemistry in this kinesin-6. *Open Biol.* **13**, 230122 (2023).
94. J. Locke *et al.*, Structural basis of human kinesin-8 function and inhibition. *Proc. Natl. Acad. Sci. U.S.A.* **114**, E9539–E9548 (2017).
95. J. Xing, K. Schindler, Genetic variants from whole exome sequencing of female IVF patients. Rutgers University Community Repository (RUcore). https://scholarship.libraries.rutgers.edu/esploro/outputs/99103196430410464 6. Deposited 1 July 2024.

Downloaded from https://www.pnas.org by 188.129.80.218 on July 30, 2025 from IP address 188.129.80.218.